Basic Res Cardiol (2013) 108:328
DOI 10.1007/s00395-013-0328-2

ORIGINAL CONTRIBUTION

Rapid binding of electrostatically stabilized iron oxide nanoparticles to THP-1 monocytic cells via interaction with glycosaminoglycans

Antje Ludwig · Wolfram C. Poller · Kera Westphal · Susann Minkwitz · Gisela Lättig-Tünnemann · Susanne Metzkow · Karl Stangl · Gert Baumann · Matthias Taupitz · Susanne Wagner · Jörg Schnorr · Verena Stangl

Received: 23 April 2012 / Revised: 18 December 2012 / Accepted: 20 December 2012 / Published online: 12 January 2013
© Springer-Verlag Berlin Heidelberg 2013

Abstract Magnetic resonance imaging (MRI) with contrast agents that target specific inflammatory components of atherosclerotic lesions has the potential to emerge as promising diagnostic modality for detecting unstable plaques. Since a high content of macrophages and alterations of the extracellular matrix are hallmarks of plaque instability, these structures represent attractive targets for new imaging modalities. In this study, we compared in vitro uptake and binding of electrostatically stabilized citrate-coated very small superparamagnetic iron oxide particles (VSOP) to THP-1 cells with sterically stabilized carboxydextran-coated Resovist®. Uptake of VSOP in both THP-1 monocytic cells and THP-derived macrophages (THP-MΦ) was more efficient compared to Resovist® without inducing cytotoxicity or modifying normal cellular functions (no changes in levels of reactive oxygen species, caspase-3 activity, proliferation, cytokine production). Importantly, VSOP bound with high affinity to the cell surface and to apoptotic membrane vesicles. Inhibition of glycosaminoglycan (GAG) synthesis by glucose deprivation in THP-MΦ was associated with a significant reduction of VSOP attachment suggesting that the strong interaction of VSOP with the membranes of cells and apoptotic vesicles occurs via binding to negatively charged GAGs. These in vitro experiments show that VSOP-enhanced MRI may represent a new imaging approach for visualizing high-risk plaques on the basis of targeting pathologically increased GAGs or apoptotic membrane vesicles in atherosclerotic lesions. VSOP should be investigated further in appropriate in vivo experiments to characterize accumulation in unstable plaque.

Keywords Magnetic resonance imaging · Iron oxide particles · Macrophages · Cytotoxicity · Glycosaminoglycans · Atherosclerosis

A. Ludwig (✉) · W. C. Poller · K. Westphal · S. Minkwitz · S. Metzkow · K. Stangl · G. Baumann · V. Stangl
Medizinische Klinik mit Schwerpunkt Kardiologie und Angiologie, Charité, Universitätsmedizin Berlin, Campus Mitte, Charitéplatz 1, 10117 Berlin, Germany
e-mail: antje.ludwig@charite.de

V. Stangl
e-mail: verena.stangl@charite.de

G. Lättig-Tünnemann
Center for Stroke Research Berlin, Charité, Universitätsmedizin Berlin, Campus Mitte, Charitéplatz 1, 10117 Berlin, Germany

M. Taupitz · S. Wagner · J. Schnorr
Institut für Radiologie, Charité, Universitätsmedizin Berlin, Campus Mitte, Charitéplatz 1, 10117 Berlin, Germany

Introduction

Macrophages are central players in various infectious and inflammatory diseases, such as rheumatoid arthritis, multiple sclerosis and atherosclerosis. They produce cytokines and chemokines that are critically important in the initiation and maintenance of inflammation [11]. In atherosclerotic plaques, high numbers of macrophages are a hallmark of plaque instability, since they secrete inflammatory mediators causing alterations of the extracellular matrix thereby destabilizing the plaque [12, 15, 35]. Consecutive degradation of collagens and changes in composition of proteoglycans and their GAG chains, as well as cell death and the appearance of extracellular membrane particles contribute to plaque instability [5, 6, 10, 12, 15–17]. Vulnerable plaques tend to rupture, causing life-threatening complications such as acute myocardial infarction and stroke [12, 22].

There is increasing experimental and clinical evidence that macrophages and inflammation-associated structures in plaque regions can be tagged with iron oxide nanoparticles and may thus be visualized by in vivo MRI [2, 7, 14]. In particular, superparamagnetic iron oxide particles (SPIO) and ultrasmall superparamagnetic iron oxide particles (USPIO) are suitable for detection of early inflammatory stages of atherosclerotic lesions [2, 7, 23–25, 29, 30, 31, 33, 34, 36]. (U)SPIO-enhanced MRI may be useful for monitoring the response to anti-inflammatory treatment as well. Thus, atorvastatin therapy has been shown to significantly reduce USPIO-enhanced MRI-defined plaque inflammation after 6 and 12 weeks of treatment [30]. Despite the promising potential of MRI using dextran-coated (U)SPIO with regard to characterization of vascular wall anatomy and plaque composition, some challenging issues need to be overcome before this technique can be translated into clinical practice. First, all (U)SPIO variants can be detected at the earliest 24 h after injection. Second, potential cytotoxicity of iron oxide nanoparticles remains an issue of debate [26].

Experimental and clinical data suggest that electrostatically stabilized citrate-coated very small superparamagnetic iron oxide particles (VSOP) may have some advantages over conventional sterically stabilized (U)SPIO [32, 38]. VSOP are significantly smaller ($\sim$7 nm) and its cellular uptake is faster and quantitatively superior compared to polymer-coated iron oxide nanoparticles [32]. VSOP are the only electrostatically stabilized iron oxide crystals that have entered the clinical development up to phase II trials as a contrast agent for MRI [37].

Since macrophages and alterations of the extracellular matrix are a hallmark of plaque instability and therefore attractive targets for new imaging modalities, the aim of our study was to compare in vitro uptake and binding mechanisms of electrostatically stabilized VSOP to these structures with sterically stabilized SPIO Resovist®. We used human myelomonocytic cell line THP-1, which is not only suitable to study monocyte/macrophage biology in cell culture systems but is also characterized by high expression and secretion of the large matrix proteoglycans versican and perlecan [13]. Beyond investigation of the interaction of VSOP with monocytes, proteoglycans and their GAG chains, putative toxic effects of these citrate-coated nanoparticles and the impact of their accumulation on the range of functions and signaling pathways were investigated.

Methods

Reagents

Unless otherwise stated, all chemicals and solvents were purchased from Sigma-Aldrich, Germany. Resovist® was purchased from Bayer Schering Pharma (Berlin, Germany). VSOP was manufactured according to the patent by Pilgrimm [20] and were finally adjusted to a 0.5 M iron concentration with 13 % citric acid (weight/weight total iron), 3 g/l sodium glycerophosphate, 2 g/l *N*-methylglucamine, and 60 g/l mannitol, which was adapted to the final pharmaceutical formulation of the investigational drug VSOP-C184, batch 050701 used in clinical trials. Characteristics of VSOP: hydrodynamic diameter, 8.1 $\pm$ 4 nm; relaxivity r1, 19; relaxivity r2, 56.

Cell culture conditions and treatment with particles

THP-1 cells (human acute monocytic leukemia cell line) are widely used to study monocyte/macrophage biology in cell culture systems. Cells were obtained from the ATCC (Wesel, Germany), cultured in suspension in RPMI medium 1640 (Invitrogen, Germany), and supplemented with 10 % fetal calf serum (FCS, Biochrom, Germany), 100 U/ml penicillin, 100 µg/ml streptomycin (Invitrogen), and either with or without 2 mM L-glutamine (Invitrogen). For indicated experiments, THP-1 cells were cultured in medium without glucose for 12–16 weeks. For differentiation into macrophages, THP-1 monocytic cells (THP-Mo) were treated for 72 h with 20 ng/ml phorbol myristate acetate (PMA), and washed three times with medium afterwards. After 24 h of rest, the resulting macrophages (THP-MΦ) were used for experiments. Primary human macrophages (MΦ) were prepared as follows: Buffy coats of healthy volunteers were purchased from the DRK Blutspendedienst (Germany). Ethical approval was obtained from the Ethics Committee of Charité Universitätsmedizin Berlin. Peripheral blood monocytic cells were isolated by Ficoll/Paque (Biochrom, Germany) density gradient centrifugation. Cells were resuspended in serum-free RPMI 1640 medium and allowed to adhere (1×10^7 cells/well) in 6-well plates in a final volume of 2 ml. After 1 h incubation at 37 °C, non-adherent cells were removed by three times washing with medium. Macrophages were obtained after cultivation in RPMI 1640 with 10 % FCS and recombinant macrophage colony stimulating factor (10 ng/ml) for 7 days. Treatments were performed in medium with 1 % FCS to avoid interaction of iron oxide nanoparticles with serum proteins. An iron concentration of 0.75 mM (41 µg/ml) was selected, corresponding to the serum iron concentration observed in a phase I clinical trial at an intermediate dose of 0.045 mmol Fe/kg, which is the intended dose for clinical use as a contrast agent for magnetic resonance angiography [32].

Determination of iron concentration

THP-Mo were cultured in flasks with a density of 1×10^6 cells/ml in medium. Following incubation with

iron oxide nanoparticles, aliquots of cells were counted in a hemocytometer, centrifuged for 5 min at 200*g*, and washed three times with PBS. Pellets were resuspended in 20 µl of 35 % (10 N HCl), and afterwards 1 ml H_2O_{dest} was added to the suspension. Samples were centrifuged for 5 min at 5,000*g* to remove cellular debris. Aliquots of 50 µl of the supernatant were mixed with 50 µl of reagent A (1.5 M hydroxylamine hydrochloride) and 150 µl reagent B (4 mM 1,10-phenanthroline hydrochloride, 200 mM acetic acid, 160 mM sodium acetate). Absorbance of samples was measured using an AnthosIII (Biochrom, Germany) microplate reader at 492 nm. Iron concentrations were calculated using internal standard curves of iron standard Titrisol (Merck, Germany). THP-MΦ were differentiated and cultivated in dishes (diameter 6 cm) with a density of 1×10^6 cells in 2 ml of medium. Following incubation, cells were detached by scraping, if necessary, and an aliquot was used to determine the exact cell number in a hemocytometer. Cells were washed three times with PBS and centrifuged for 5 min at 200*g*. Pellets were processed as described above.

Cell viability and proliferation

Following 24 h incubation with iron oxide nanoparticles, THP-Mo were washed and seeded at 1×10^6 cells in 5 ml medium supplemented with 10 % FCS in T25 flasks (BD Falcon, Heidelberg, Germany). Cell count was n_1 at $t_1 = 0$ h. Cells were cultured for additional 7 days. To estimate the mean population doubling time, the cell count at day 7 was defined as n_2 at $t_2 = 168$ h. Doubling time (t_D) was calculated as $t_D = \log 2\ (t_2 - t_1)/(\log\ n_2 - \log\ n_1)$. Trypan blue staining was used to determine the proportion of nonviable cells.

Detection of reactive oxygen species and caspase-3 activity

The level of intracellular reactive oxygen species (ROS) was measured using 2′,7′-dichlorofluorescein diacetate (DCF) as described previously [18].

Caspase-3 activity was determined using the fluorescence substrate Ac-Asp-Glu-Val-Asp-7-amido-4-methyl coumarin (Ac-DEVD-AMC). THP-Mo were counted, and exactly 2×10^5 cells were lysed in PBS containing 1 % triton-X100 for 10 min on ice. After centrifugation, the cleared lysate was mixed with 50 µl reaction buffer containing 40 mM hepes (pH 7.5), 40 % glycerol, 8 mM DTT, and 2 mM Ac-DEVD-AMC. Release of fluorescent AMC was monitored in a fluorescence plate reader (GeminiEM, Molecular Devices, Germany) at an excitation wavelength of 380 nm and an emission wavelength of 450 nm. The increase in fluorescence during 2 h was calculated and used as arbitrary units of caspase-3 activity. Caspase-3 activity of iron oxide nanoparticle-treated cells was expressed as relative activity compared to control.

Cytokine assays

After treatment with iron oxide nanoparticles, THP-1-derived macrophages (THP-MΦ) were washed and transferred to fresh medium. Treatment with low-dose lipopolysaccharide (LPS, 5 ng/ml) was used for induction of cytokine production. After 24 h, culture supernatants were collected and centrifuged at 4 °C for 5 min at 2,000*g* in order to remove any detached cells. Supernatants were transferred to fresh tubes and stored at −20 °C until analysis. Levels of interleukin-6 (IL-6), tumor necrosis factor-α (TNF-α), interferon-inducible T-cell alpha chemoattractant-1 (ITAC-1), and monocyte chemotactic protein 1 (MCP-1) were determined using commercially available enzyme-linked immunosorbent assays (R&D Systems, Germany) according to the suppliers' instructions.

Microscopy and staining

For microscopy, 1×10^6 THP-Mo were spotted on glass slides and THP-MΦ were cultured on cover slips. After treatment with iron oxide nanoparticles, cells were washed and iron was detected by Prussian blue staining (2 % potassium ferrocyanide in 1 % HCl) followed by counterstain with Nuclear Fast Red. Commercial kit for Alcian blue-PAS staining (Merck, Germany) was used to visualize GAGs according to the manufacturer's protocol.

Quantification of GAG in cell culture supernatants

THP-Mo were seeded at a density of 1×10^5 cells per ml in cell culture medium with or without glucose and supplemented with 1 % of FCS. After 24 h, 50 µl of the cell culture supernatant was collected and centrifuged to eliminate cellular debris. The content of GAGs was determined by precipitation with alcian blue as described by Whiteman [39]. Alcian blue was released from precipitates by treatment with 200 µl of 2 % SDS, and optical density at 620 nm was determined in a spectrophotometer (Beckman, Germany).

Chondroitinase ABC treatment

After treatment with iron oxide nanoparticles, THP-MΦ ($\sim 5 \times 10^5$ cells in 6 cm petri dishes) were thoroughly washed with PBS and incubated for 30 min at 37 °C with 0.5 U of chondroitinase ABC (ChABC) from *Proteus vulgaris* in 1 ml ChABC reaction buffer [50 mM Tris (ph 8.0), 60 mM Na-acetate]. Supernatant and cells were

separately collected. Cells were scraped and centrifuged. Supernatant was evaporated to a volume of 20 µl. The iron content in the supernatant and in cell pellets was determined as described above.

Electron microscopy

For electron microscopy, THP-Mo and THP-MΦ were treated for the indicated times with nanoparticles, centrifuged and washed twice in PBS. Cells were fixed with 1.5 % formaline and 2.5 % glutaraldehyde in PBS for 15 min. After several washes with PBS, the cells were post-fixed in 4 % osmium tetroxide in 0.1 M phosphate buffer (pH 7.4) for 60 min and washed 3 times in PBS. Cell pellets were dehydrated in graded series of ethanol, transferred into propylene oxide, and incubated overnight in preembedding solution [55 g of araldite and DDSA (dodecenyl succinic anhydride, araldite hardener) mixed in a ratio of 30:24; 1.5 ml DMP-30 (2,4,6-trisdimethylaminomethyl-phenol, epoxy accelerator, both Serva, Germany) and 50 ml propylene oxide]. The next day, pellets were incubated 2 × 2 h in the embedding solution (100 g of araldite and DDSA mixed in a ratio of 30:24 and 2 ml DMP-30) and finally embedded in the cap of an Eppendorf tube (Eppendorf, Germany). Resin was polymerized for 24–60 h at 65 °C. Ultrathin sections (70 nm) were cut using an ultramicrotome (Leica, Germany) with a diamond knife (Diatome, Switzerland). Ultrathin sections were collected on 300-mesh nickel grids (Plano, Germany) and stained with uranyl acetate and lead citrate. Electron microscopy was performed on a Leica EM 900 (Leica, Germany). The images were acquired with the integrated camera (Leica, Germany).

Isolation of THP-1-derived apoptotic debris and membrane vesicles

THP-Mo were treated with TNF-α (10 ng/ml) and actinomycin D (0.5 µg/ml) for 16 h in medium without FCS to induce apoptosis. Medium was clarified from intact cells by centrifugation (800*g*, 10 min). The supernatant containing apoptotic debris and membrane vesicles (AMV) was further centrifuged (12,000*g*, 20 min). The pelleted AMV were suspended in medium. For quantification, the protein content of AMV was estimated by bicinchoninic acid protein assay (Pierce Biotechnology, USA).

Magnetic resonance imaging

Labeled and washed 1×10^6 cells or AMV were embedded in 50 µl of 1 % low-melting point agarose (BRL, USA) and imaged on a clinical 1.5 T MR scanner (Siemens Sonata, Germany using a commercially available wrist coil). Cell agarose mixture was cooled in 1.5 ml Eppendorf vials and additionally embedded in surrounding low-melting point agarose to fix them in upright position in a container fitting in outer dimensions to the wrist coil. Imaging was performed in frontal section orientation with 1.5 mm slice thickness using a T2*-weighted 2D gradient echo (GRE) sequence (TR 200 ms/TE 6 ms/FA 20°) with an in-plane resolution of 0.5 × 0.5 mm.

Results

Uptake of iron oxide nanoparticles by THP-1 cells

Figure 1 shows the iron uptake of VSOP in THP-Mo, THP-MΦ and primary human MΦ compared to the uptake of the carboxydextran-coated Resovist®. Both THP-Mo and THP-MΦ had taken up VSOP faster than Resovist®. In general, THP-MΦ and primary human MΦ had taken up more particles than THP-Mo. After 24 h of treatment of THP-Mo, the measured iron content was 2.1 ± 0.5 pg/cell for Resovist® and 19.6 ± 5.1 pg/ml for VSOP. In THP-MΦ, iron content after 24 h treatment was 18.2 ± 1.1 pg/cell for Resovist®, and 51.9 ± 2.2 pg/cell for VSOP. In primary human MΦ, iron content after 24 h treatment was 22.6 ± 0.3 pg/cell for Resovist® and 60.3 ± 7.4 pg/cell for VSOP.

Agarose phantom MRI allowed the estimation of the qualitative visible signal lowering effect in relation to the quantitative iron concentration. There was an optimal range between 2.5 and 5 pg iron per cell with 2×10^7 cells per ml, so that a signal loss was already observed within 1 h of incubation with VSOP in THP-Mo as well as in THP-MΦ. Higher cellular iron concentrations led to disturbances in local magnetic fields, resulting in bright and dark areas with spatial distortion of the shape of the test tubes (Fig. 1, lower panel).

Effect of cell-associated iron oxide nanoparticles on cellular function

There was no increase in ROS content between control cells and cells treated with VSOP or Resovist® (Fig. 2a). Also, loading with iron oxide nanoparticles did not cause a measurable increase in caspase-3 activity in THP-Mo (Fig. 2b).

No significant differences in proliferation characteristics were observed between unloaded cells and cells loaded either with Resovist® or VSOP (Fig. 2c). The proportion of trypan-blue-positive cells was unchanged by the loading and was approximately 4 %.

Figure 3a shows that iron oxide nanoparticle loading of THP-MΦ had no effect on the basal production of IL-6,

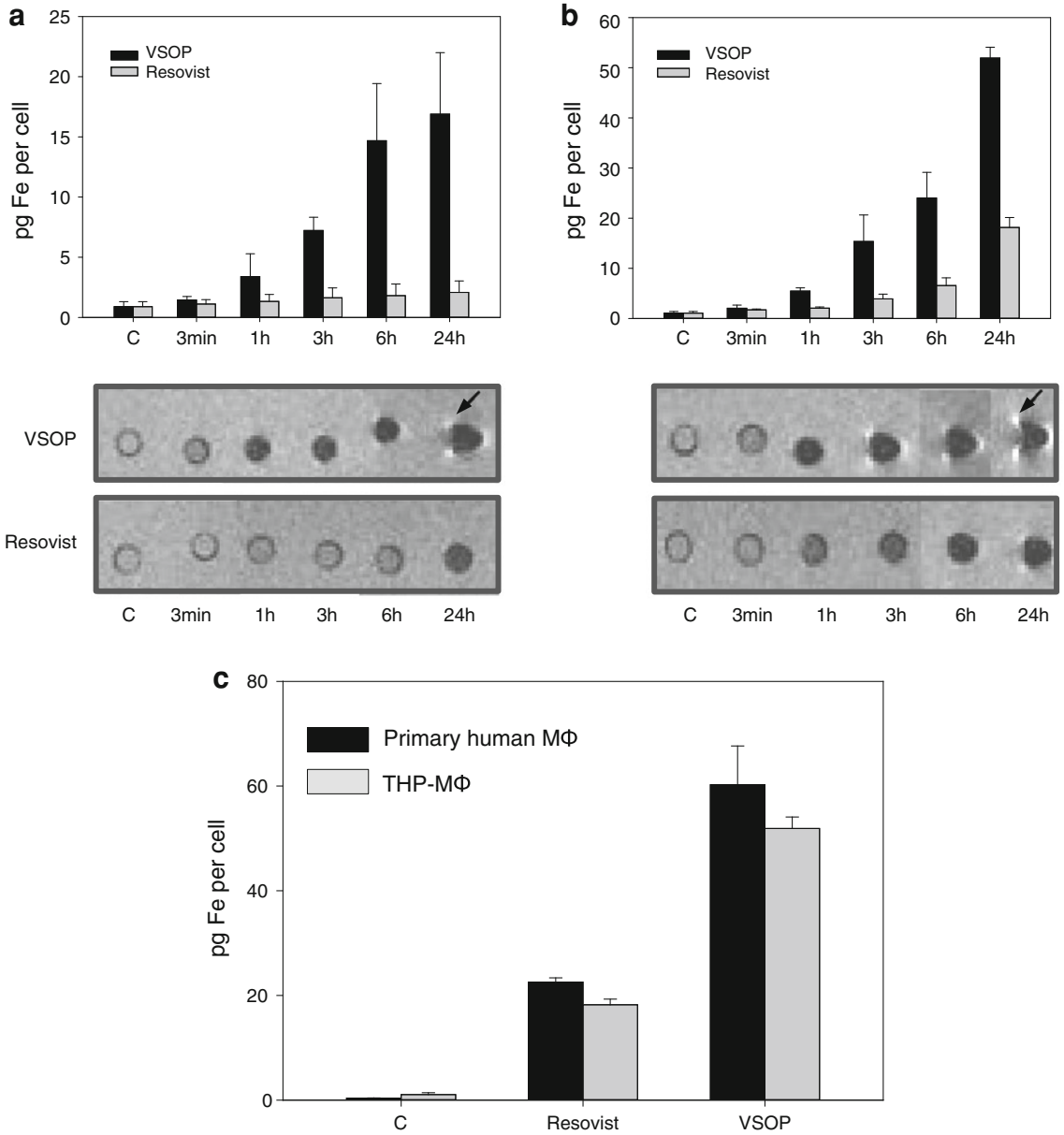

Fig. 1 Uptake of iron oxide nanoparticles in THP-1 cells and primary human macrophages. **a** THP-Mo and **b** THP-MΦ were incubated with 0.75 mM VSOP or Resovist® for the indicated times. The content of cell associated iron was determined colorimetrically by the phenanthroline method. Data are presented as means of three independent experiments ± standard deviation (SD). Control (C) = unloaded cells. *Lower panels* show MR images of agarose embedded THP-Mo and THP-MΦ after treatment with 0.75 mM VSOP and Resovist® for the indicated times. High cellular iron concentrations lead to disturbances in local magnetic fields, resulting in bright and dark areas with spatial distortion (*arrows*). **c** Primary human MΦ were prepared from buffy coat of healthy blood donors. Cells were incubated with 0.75 mM VSOP or Resovist® for 24 h. The content of cell associated iron was determined colorimetrically by the phenanthroline method and compared to the content of cell associated iron of THP-MΦ after 24 h incubation with 0.75 mM VSOP or Resovist®. Data are presented as means of three independent experiments ± standard deviation (SD). Control (C) = unloaded cells

ITAC-1, and MCP-1. A slight increase in TNF-α secretion was detectable in VSOP-loaded THP-MΦ (Fig. 3a). In contrast, LPS treatment induced a strong increase in the production of all four cytokines in THP-MΦ. LPS-stimulated cytokine secretion was not significantly affected by preloading with iron oxide nanoparticles (Fig. 3b).

Localization of cell-associated iron oxide nanoparticles

Images of light microscopy of cells loaded for 24 h with iron oxide nanoparticles after Prussian blue staining and nuclear fast red staining are shown in Fig. 4a. Light microscopy revealed that VSOP were not only located

within the cytoplasm of monocytes and macrophages but are bound to a large extent onto the cell surface, whereas Resovist® was exclusively located within THP-MΦ, as expected, but was hardly detectable inside monocytes. Remarkably, VSOP were also detectable in extracellular aggregates. Electron microscopy provided further insights into the different uptake modalities of VSOP and Resovist®. As shown in Fig. 4b, after 24 h incubation Resovist® particles were mainly localized inside few densely packed intracellular vesicles in THP-Mo. Compared to Resovist®, VSOP were found in considerable higher quantity in densely packed vesicles as well as in large loosely packed internal structures in THP-Mo. Moreover, aggregates of VSOP accumulated on the surface of the cell. As expected, compared to THP-Mo, in THP-MΦ, higher amounts of cell-associated particles were detectable, even after a short

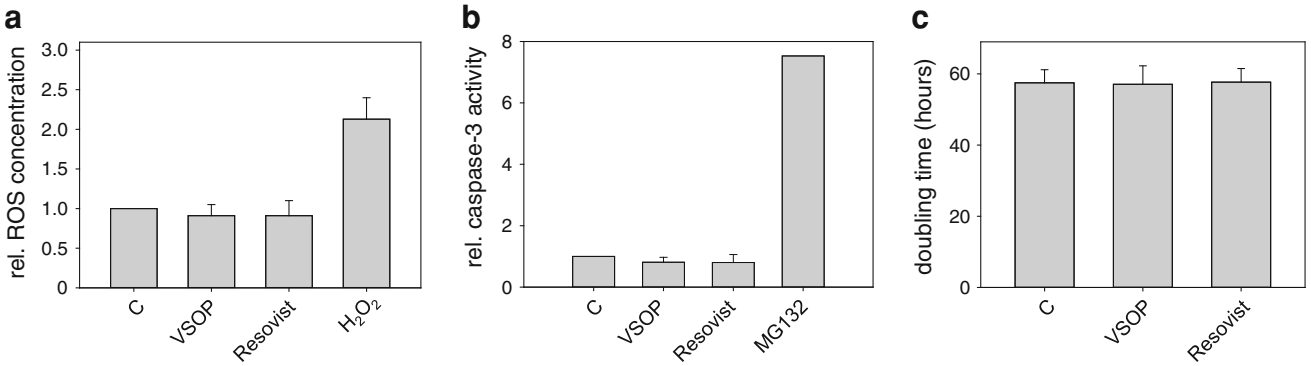

Fig. 2 Influence of iron oxide nanoparticles on the cell function of THP-1 monocytes THP-Mo were either treated with 0.75 mM VSOP or Resovist® for 24 h. The influence of cell associated particles on **a** intracellular ROS measured by the determination of DCF fluorescence, **b** the activity of caspase-3 determined fluorimetrically using the substrate Ac-Asp-Glu-Val-Asp-7-amido-4-methyl coumarin (Ac-DEVD-AMC), and **c** on proliferation (represented as doubling time of the cell population). As positive control for the increase of intracellular ROS a 30 min treatment with 500 μM H_2O_2 and for caspase-3-activation a 24 h treatment with the proteasome inhibitor MG132 in a concentration of 1 μM was used. Data are presented as means from three independent experiments ± standard deviation (SD). Control (C) = unloaded THP-Mo

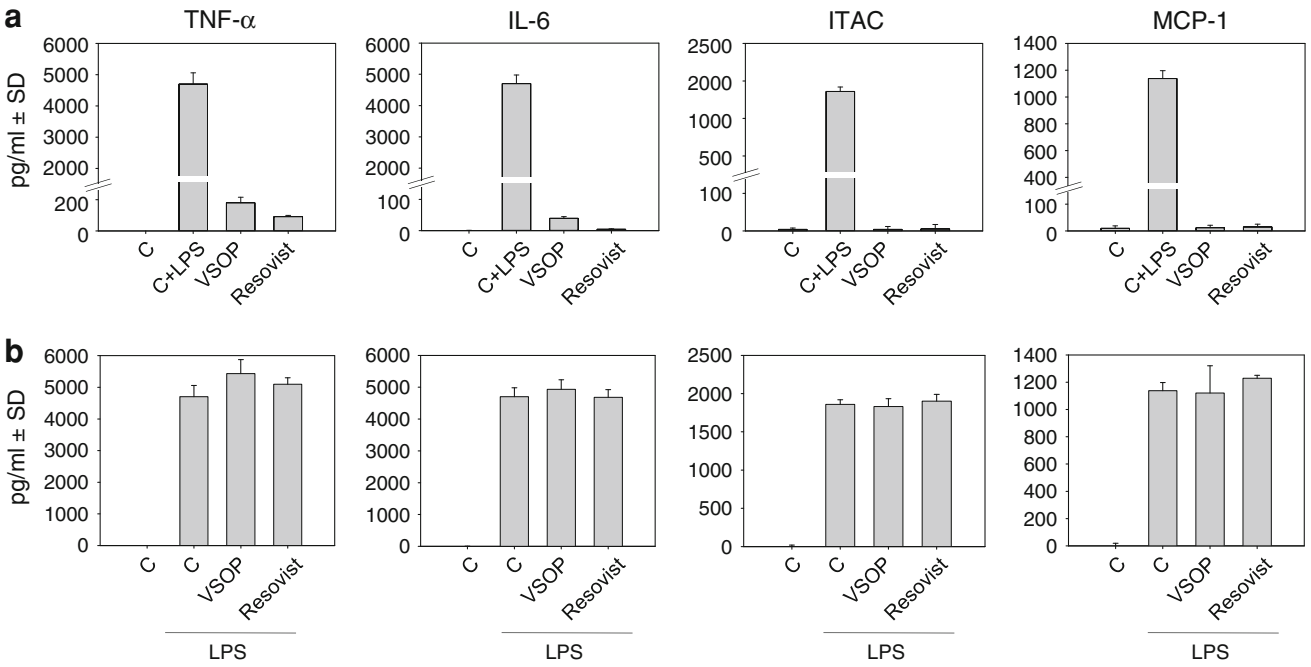

Fig. 3 Influence of iron oxide nanoparticles on the cytokine secretion of THP-1 macrophages THP-MΦ were treated for 24 h with either 0.75 mM VSOP or Resovist®. Untreated THP-MΦ served as a control (C). After treatment the loaded macrophages were washed and incubated for further 24 h with medium alone (**a**) or under stimulation with 5 ng/ml LPS (**b**) and the cytokine concentration in the medium was measured by ELISA. Cytokine concentrations were calculated using internal standard curves and results are expressed as means of three experiments ± SD

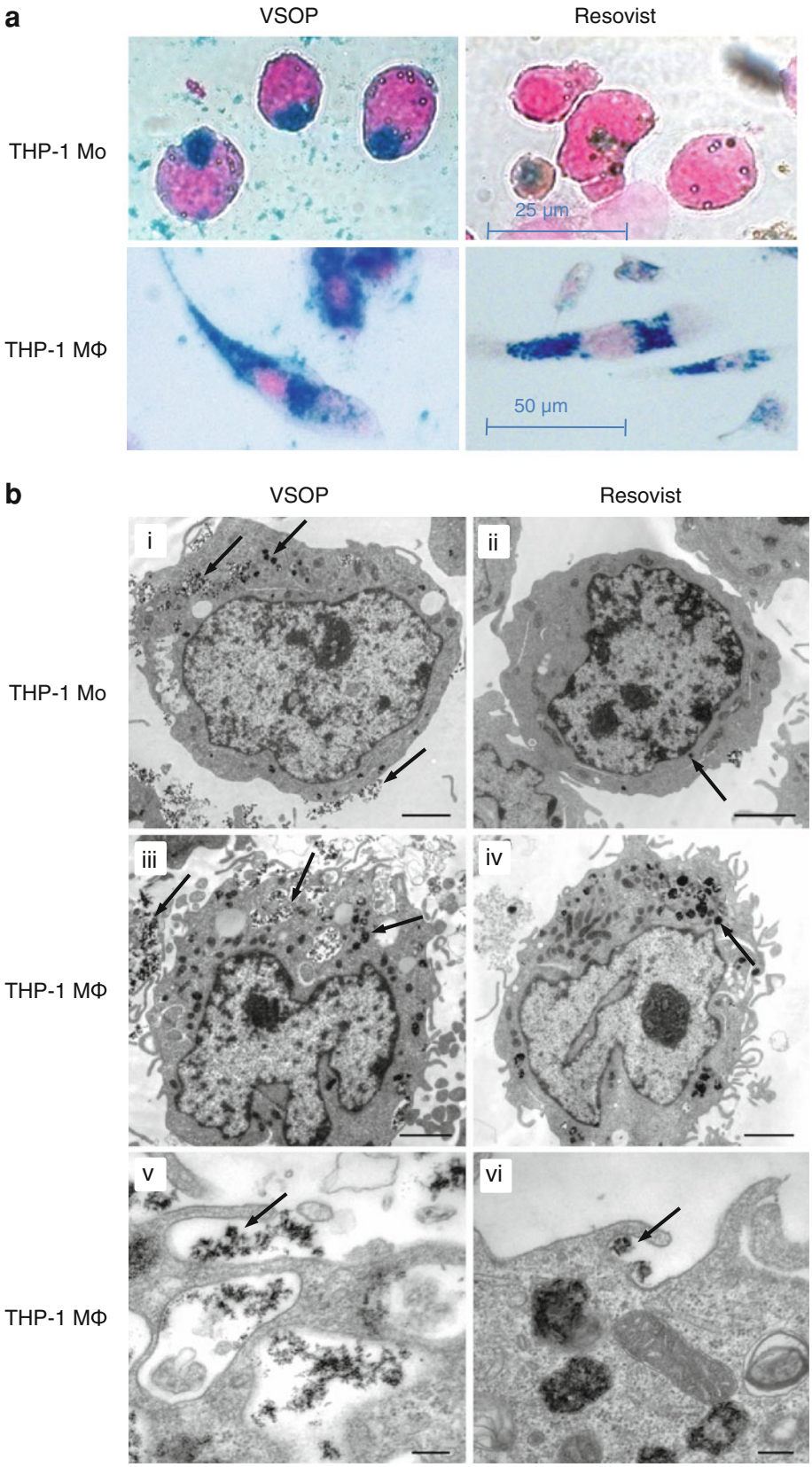

Fig. 4 Localization of iron oxide nanoparticle in THP-1 cells. **a** Images of light microscopy of THP-Mo and THP-MΦ after 24 h treatment with 0.75 mM VSOP and Resovist®. Nuclei were visualized with Nuclear Fast Red staining and cell associated iron by Prussian Blue staining. **b** Transmission electron micrographs of ultrathin sections THP-1 cells incubated with 0.75 mM VSOP and 0.75 mM Resovist for 24 h (THP-Mo; **i**, **ii**) or 4 h (THP-MΦ, **iii**–**vi**). Electron dense inclusions and extracellular aggregates represent cell associated iron oxide nanoparticles (*arrows*). *Size bars* **i**–**iv** 2 µm; **v**, **vi** 200 nm

incubation time of 4 h. Again, Resovist® was exclusively located within vesicles, whereas VSOP were found in large loosely packed structures and densely packed vesicles as well as in aggregates on the cell surface. In THP-MΦ, ongoing phagocytosis of aggregated particles (VSOP and Resovist®) were frequently visible (Fig. 4b, v and vi).

Binding of VSOP to extracellular structures

It is known that THP-1 cells express large matrix proteoglycans [13]. Therefore, we tested the hypothesis that aggregation of VSOP on the surface of THP-1 cells is mediated by GAG chains of these proteoglycans. Since it has recently been shown that glucose deficiency inhibits the synthesis of GAG in fibroblast cultures [1], we cultured THP-1 cells in medium without glucose for 12–16 weeks. Alcian blue-PAS staining of THP-MΦ showed that withdrawal of glucose in fact decreased the amount of alcian-blue-positive cellular structures (Fig. 5a). In addition, the concentration of GAGs secreted by THP-MΦ into the culture medium was significantly decreased after glucose withdrawal as revealed by the measurement of insoluble complexes formed with alcian blue (Fig. 5b). Figure 5c shows that glucose deprivation decreased the level of cell-associated iron in THP-MΦ compared to THP-MΦ cultivated with 0.6 % glucose after incubation with VSOP, whereas uptake of Resovist® was unchanged. Moreover, treatment of iron oxide particle loaded THP-MΦ with ChABC revealed that a large proportion of cell-associated VSOP bound to ChABC-sensitive structures on the cell surface. After 24 h incubation with VSOP, 22.4 ± 4.9 % of cell-associated iron was removed from the cells by ChABC treatment (Fig. 5d). Interestingly, after a shorter incubation time of 3 h, the proportion of ChABC-sensitive cell bound iron was almost 50 %, albeit the overall content of cell-associated iron was naturally lower. Cell-associated Resovist® is insensitive to ChABC treatment (Fig. 5d).

Binding of VSOP to apoptotic debris and membrane vesicles

Treatment of THP-1 with TNF-α and actinomycin-D resulted in the formation of apoptotic debris and membrane vesicles (AMV). VSOP bound within minutes to in vitro generated THP-1-derived AMV. After 5 min incubation with VSOP, the concentration of bound iron was 17.53 ± 0.39 pg/pg protein. The iron concentration reached 24.76 ± 1.23 pg/pg protein after 15 min incubation and was not further increased with longer incubation time (Fig. 6a). Notably, incubation with 1.5 mM VSOP did not increase the amount of bound iron compared to incubation with 0.75 mM VSOP (Fig. 6b). Electron micrographs shown in Fig. 6c illustrate several apoptotic membrane vesicles surrounded by apoptotic debris. These membrane vesicles have a medium size of 200–300 nm and partially contain degraded cellular organelles. As expected, no phagocytosis was present and the vesicle membranes showed gaps of up to 300 nm. No VSOP were detectable within the vesicles but aggregated on the outside of the vesicle membranes.

Discussion

The central findings of the present study are, first, that citrate-coated VSOP are not only incorporated intracellularly in THP1-monocytes and THP1-derived macrophages but also bind with high affinity to the extracellular surface and to negatively charged GAGs as well as to AMV; second, that binding of VSOP in vitro occurs much faster than binding of carboxydextran-coated USPIO Resovist®; and, third, that the accumulation of VSOP affects neither cellular functions nor homeostasis and is not associated with toxic effects for the cells.

In this study, we compared in vitro uptake and binding of electrostatically stabilized citrate-coated VSOP to THP-1 cells with sterically stabilized carboxydextran-coated Resovist®.The observation that VSOP label THP-Mo and THP-MΦ much faster and more effectively than Resovist® indicates differences in the uptake modalities between both iron oxide nanoparticles. The more effective uptake of VSOP compared to Resovist® was confirmed in primary human MΦ, showing that potent labeling with VSOP is not limited to oncogenically transformed monocytic cells. Light and electron microscopy revealed that in contrast to Resovist® which is incorporated into vesicles inside cells by phagocytosis, VSOP are not only exclusively located within cellular vesicles but also detectable on the cellular surface and in extracellular aggregates. Recently, it was communicated that artificial pre-aggregation of gold nanoparticles leads to extremely high loading of cells with gold due to elevated phagocytosis [9]. We suggest that particle aggregation on the cell surface highly promotes phagocytosis of VSOP. Therefore, the rapid and effective binding of VSOP can be attributed first to the rapid attachment to the cell surface, and then to an enhanced phagocytosis of surface bound aggregates.

Since synthesis of large amounts of membrane-bound and extracellular proteoglycans is characteristic of THP-1 cells [13], we hypothesized that VSOP have high affinity for these complex macromolecules and that these glycosylated molecules act as mediators for rapid intracellular uptake. The fact that inhibition of GAG synthesis by glucose deprivation [1] in THP-MΦ was associated with significant reduction in VSOP binding, whereas Resovist® uptake remained unchanged, clearly supports this hypothesis. The chondroitin sulfate proteoglycan versican in its isoforms V0 and V1 is

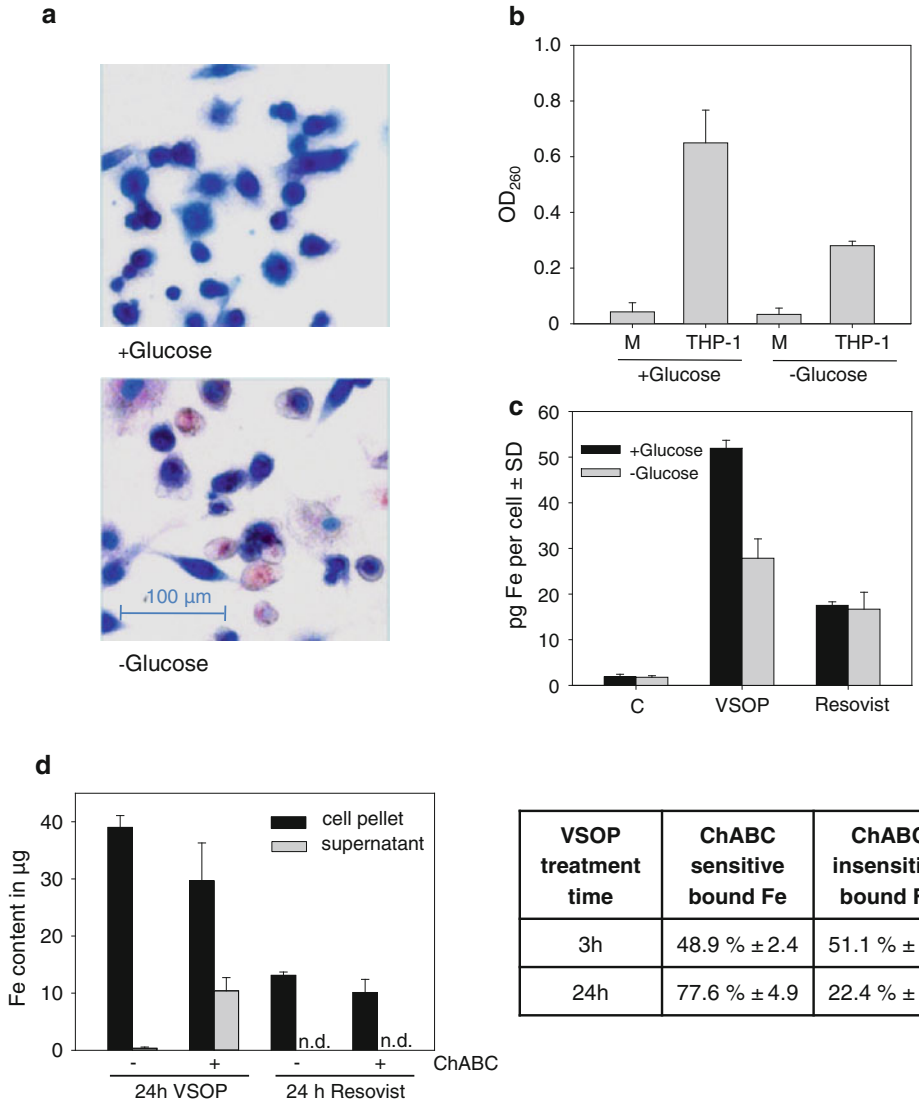

VSOP treatment time	ChABC sensitive bound Fe	ChABC insensitive bound Fe
3h	48.9 % ± 2.4	51.1 % ± 2.4
24h	77.6 % ± 4.9	22.4 % ± 4.9

Fig. 5 Influence of glucose withdrawal on the uptake of iron oxide nanoparticles in THP-1 cells. **a** Images of light microscopy of THP-MΦ cultivated either in glucose-containing medium (*upper panel*) or in glucose-free medium (*lower panel*), after alcian blue-PAS staining. **b** Photometric determination of alcian blue released from complexes formed with glycosaminoglycans in the cell culture medium of THP-MΦ cultivated either in glucose-containing medium or in glucose-free medium. *M* cell free cell culture medium. **c** THP-MΦ cultivated either in glucose-containing medium (*black bars*) or in glucose-free medium (*grey bars*), were treated for 24 h with 0.75 mM VSOP or Resovist®. The content of cell associated iron was determined colorimetrically by the phenanthroline method. Data are presented as means from three independent experiments ± standard deviation (SD). Untreated THP-MΦ served as control. **d** Graph: THP-MΦ were treated for the indicated times with either 0.75 mM VSOP or Resovist®. Adherent cells were treated with chondroitinase ABC (ChABC) or ChABC reaction buffer alone and the iron content was measured in the supernatant and in cells colorimetrically by the phenanthroline method. The table shows the percentage of cell associated iron bound to ChABC sensitive structures on the cell surface (ChABC sensitive bound iron) and the percentage of iron bound to ChABC insensitive cellular structures (ChABC insensitive bound iron) after the indicated times of treatment with 0.75 mM VSOP. Data are presented as means from three independent experiments ± standard deviation (SD)

dominantly expressed in THP-1 cells [13]. In fact, a large proportion of cell surface-bound VSOP is removable by chondroitinase ABC treatment. This enzyme preferentially cleaves chondroitin sulfates A, B, and C and at lesser rates chondroitin and hyaluronic acid [40], indicating that these structures are involved in the binding and aggregation of VSOP on the cell surface of THP-1 cells.

Another argument in favor of VSOP affinity for GAG is that VSOP are very rapidly trapped by in vitro generated THP-1-derived apoptotic debris, including apoptotic membrane vesicles, which are structures disabled for phagocytosis. Vats et al. have shown strong interaction between citrate-coated iron oxide nanoparticles and endothelial cell-derived microparticles shed by human umbilical

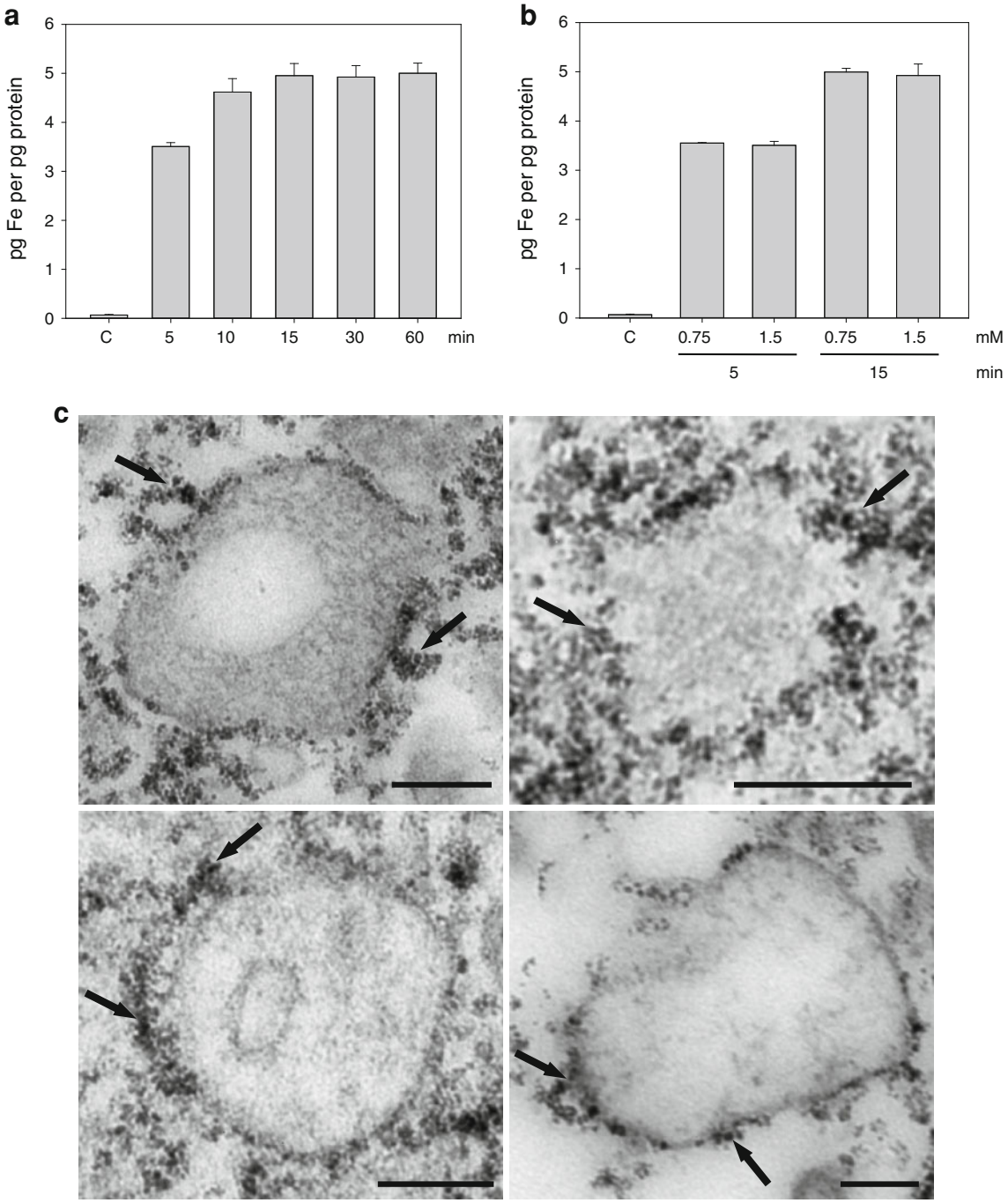

Fig. 6 Binding of iron oxide nanoparticles to THP1-derived apoptotic debris and membrane vesicles. **a** Uptake kinetic of VSOP in THP1-derived derived apoptotic debris and membrane vesicles (AMV). AMV were incubated with 0.75 mM VSOP for the indicated times. The content of AMV associated iron was determined colorimetrically by the phenanthroline method. **b** AMV were incubated with 0.75 and 1.5 mM of VSOP for the indicated times. The content of AMV associated iron was determined colorimetrically by the phenanthroline method. Data are presented as means from three independent experiments ± standard deviation (SD). Control (C) = unloaded THP-1-derived AMV. **c** Transmission electron micrographs of ultrathin sections of apoptotic AMV incubated with 0.75 mM for 15 min. Electron dense aggregates represent AMV associated iron oxide nanoparticles (*arrows*). *Size bar* 200 nm

vein endothelial cells (HUVEC) during stimulation with TNF-α. They related this interaction to the affinity of the anionic citrate-coated nanoparticles for cell membrane moieties of these cell-derived microparticles [36]. Since inflammatory cytokines may induce a marked increase in GAG production by HUVEC, it is worthy to discuss that binding of iron oxide particles to HUVEC-derived microparticles may also be mediated by GAGs [4]. The question

remains by which mechanisms iron oxide nanoparticles with a negatively charged surface may attach to negatively charged GAGs. GAGs have a high chelating potency resulting from the large number of carboxyl and sulfate groups, a property that has already been exploited for the development of GAG-stabilized iron oxide nanoparticles [8]. Further studies will have to show whether a trans-chelation with consecutive release of citrate is the underlying binding mechanism of VSOP to GAGs.

Potential cytotoxicity and damaging effects of free iron released from nanoparticles on cellular key activities such as proliferation and chemotaxis remain major concerns, underscoring that in-depth cytotoxic evaluation in vitro and in vivo is a basic prerequisite for further application in humans. VSOP were not toxic to monocytes and macrophages in a concentration of 0.75 mM, which corresponds to a serum level found in humans after administration of 0.045 mmol Fe/kg. VSOP caused no increase in intracellular ROS levels, no induction of apoptosis, and also no impairment of viability of THP1-cells. In addition, VSOP loading did not affect normal cell function. Key activities such as proliferation and cytokine release remained largely unaffected in VSOP-loaded THP-Mo and THP-MΦ. This is noteworthy since numerous investigators studying iron oxide nanoparticles (including VSOP) found that proliferative capacity as well as cell function and homeostasis of cultured cells were reduced, assuming that this was due to high intracellular iron concentrations [3, 27, 28]. Other studies, including ours, found iron oxide nanoparticles not to be toxic in different cell culture systems [19, 21]. These discrepancies may be due to the use of different concentrations of iron oxide particles. In addition, the iron oxide preparation used in our study was produced in a final pharmaceutical formulation which has demonstrated excellent safety data in preclinical studies [37]. Taken together, we show here that VSOP at a clinically relevant dose for potential diagnostic application and in the current pharmaceutical formulation has no considerable effects on cellular functions of THP-1 cells.

The majority of myocardial infarctions are caused by rupture of non-stenotic atherosclerotic lesions. The most common type of high-risk, prone-to-rupture plaque is the thin-cap fibroatheroma, characterized by a large lipid-rich necrotic core [15, 16, 22]. USPIO-enhanced MRI has gained prominence as an imaging modality for plaque visualization and characterization in clinical studies [2, 7, 23, 30]. Since phagocytic uptake of these nanoparticles mainly occurs by macrophages, one of the major components of vascular inflammation, USPIO MRI may have the potential to identify high-risk vulnerable plaques in vivo. As pointed out before, VSOP have the unique ability to bind to molecules of the extracellular matrix with only a portion being incorporated into cells. Matrix components such as proteoglycans serve as scaffolding for retention of lipoproteins, migration of smooth muscle cells, and accumulation of lipoprotein-loaded foam cells into the plaque, thereby contributing to atherogenesis. In addition, there are some indications that the presence of some proteoglycans also correlates with plaque instability. Thus, versican and the glycosaminoglycan hyaluronan accumulate at sites of plaque erosion and therefore have been implicated in events associated with acute coronary thrombosis [6]. Moreover, membrane vesicles shed by apoptotic cells have been associated with thrombogenicity inside plaques [5, 17]. Our data show that VSOP rapidly tag these extracellular components associated with plaque instability. As a result, we propose that VSOP-enhanced MRI may represent a new putative imaging tool for visualizing high-risk plaques on the basis of targeting pathologically increased GAGs bound to cells or accumulating outside cells in atherosclerotic lesions. Moreover, this unique property of VSOP makes them a promising candidate for investigating the role of acid GAGs in atherosclerotic plaque progression.

Acknowledgments This work was supported by the Deutsche Forschungsgemeinschaft—within the Clinical Research Unit KFO 213.

References

1. Cechowska-Pasko M, Bankowski E (2010) Glucose deficiency inhibits glycosaminoglycans synthesis in fibroblast cultures. Biochimie 92:806–813. doi:10.1016/j.biochi.2010.02.029
2. Howarth SP, Tang TY, Trivedi R, Weerakkody R, King-Im J, Gaunt ME, Boyle JR, Li ZY, Miller SR, Graves MJ, Gillard JH (2009) Utility of USPIO-enhanced MR imaging to identify inflammation and the fibrous cap: a comparison of symptomatic and asymptomatic individuals. Eur J Radiol 70:555–560. doi:10.1016/j.ejrad.2008.01.047
3. Hu F, Neoh KG, Cen L, Kang ET (2006) Cellular response to magnetic nanoparticles "PEGylated" via surface-initiated atom transfer radical polymerization. Biomacromolecules 7:809–816. doi:10.1021/bm050870e
4. Klein NJ, Shennan GI, Heyderman RS, Levin M (1992) Alteration in glycosaminoglycan metabolism and surface charge on human umbilical vein endothelial cells induced by cytokines, endotoxin and neutrophils. J Cell Sci 102:821–832
5. Kockx MM (1998) Apoptosis in the atherosclerotic plaque: quantitative and qualitative aspects. Arterioscler Thromb Vasc Biol 18:1519–1522. doi:10.1161/01.ATV.18.10.1519
6. Kolodgie FD, Burke AP, Farb A, Weber DK, Kutys R, Wight TN, Virmani R (2002) Differential accumulation of proteoglycans and hyaluronan in culprit lesions: insights into plaque erosion. Arterioscler Thromb Vasc Biol 22:1642–1648. doi:10.1161/01.ATV.0000034021.92658.4C
7. Kooi ME, Cappendijk VC, Cleutjens KB, Kessels AG, Kitslaar PJ, Borgers M, Frederik PM, Daemen MJ, van Engelshoven JM (2003) Accumulation of ultrasmall superparamagnetic particles of iron oxide in human atherosclerotic plaques can be detected by in vivo magnetic resonance imaging. Circulation 107:2453–2458. doi:10.1161/01.CIR.0000068315.98705.CC
8. Kresse M, Lawaczeck R, Pfefferer D (1995) Nanocrystalline magnetic iron oxide particles-method for preparation and use in medical diagnostics and therapy. US Patent 5427767

9. Krpetic Z, Nativo P, Prior IA, Brust M (2011) Acrylate-facilitated cellular uptake of gold nanoparticles. Small 7:1982–1986. doi:10.1002/smll.201100462
10. Kruse R, Merten M, Yoshida K, Schmidt A, Völker W, Buddecke E (1996) Cholesterol-dependent changes of glycosaminoglycan pattern in human aorta. Basic Res Cardiol 91:344–352
11. Lewis CE, McGee JO (1992) The natural immune system: the macrophage. Oxford University Press, New York
12. Libby P, Geng YJ, Sukhova GK, Simon DI, Lee RT (1997) Molecular determinants of atherosclerotic plaque vulnerability. Ann N Y Acad Sci 811:134–142. doi:10.1111/j.1749-6632
13. Makatsori E, Lamari FN, Theocharis AD, Anagnostides S, Hjerpe A, Tsegenidis T, Karamanos N (2003) Large matrix proteoglycans, versican and perlecan, are expressed and secreted by human leukemic monocytes. Anticancer Res 23:3303–3309
14. Makowski MR, Varma G, Wiethoff AJ, Smith A, Mattock K, Jansen CH, Warley A, Taupitz M, Schaeffter T, Botnar RM (2011) Noninvasive assessment of atherosclerotic plaque progression in ApoE-/- mice using susceptibility gradient mapping. Circ Cardiovasc Imaging 3:295–303. doi:10.1161/CIRCIMAGING.110.957209
15. Martinet W, Schrijvers DM, De Meyer GR (2012) Molecular and cellular mechanisms of macrophage survival in atherosclerosis. Basic Res Cardiol 107:297. doi:10.1007/s00395-012-0297-x
16. Martinet W, Schrijvers DM, De Meyer GR (2011) Necrotic cell death in atherosclerosis. Basic Res Cardiol 106:749–760. doi:10.1007/s00395-011-0192-x
17. Montoro-García S, Shantsila E, Marín F, Blann A, Lip GY (2011) Circulating microparticles: new insights into the biochemical basis of microparticle release and activity. Basic Res Cardiol 106:911–923. doi:10.1007/s00395-011-0198-4
18. Meiners S, Ludwig A, Lorenz M, Dreger H, Baumann G, Stangl V, Stangl K (2006) Nontoxic proteasome inhibition activates a protective antioxidant defense response in endothelial cells. Free Radic Biol Med 40:2232–2241. doi:10.1016/j.freeradbiomed.2006.03.003
19. Muller K, Skepper JN, Tang TY, Graves MJ, Patterson AJ, Corot C, Lancelot E, Thompson PW, Brown AP, Gillard JH (2008) Atorvastatin and uptake of ultrasmall superparamagnetic iron oxide nanoparticles (Ferumoxtran-10) in human monocyte-macrophages: implications for magnetic resonance imaging. Biomaterials 29:2656–2662. doi:10.1016/j.biomaterials.2008.03.006
20. Pilgrimm H (2007) Aqueous dispersions of superparamagnetic single domain particles production and use thereof for diagnosis and therapy. Patent PCT/EP2006/069453[WO/2007/065935]
21. Raynal I, Prigent P, Peyramaure S, Najid A, Rebuzzi C, Corot C (2004) Macrophage endocytosis of superparamagnetic iron oxide nanoparticles: mechanisms and comparison of ferumoxides and ferumoxtran-10. Invest Radiol 39:56–63. doi:10.1097/01.rli.0000101027.57021.28
22. Ross R (1993) The pathogenesis of atherosclerosis: a perspective for the 1990s. Nature 362:801–809. doi:10.1038/362801a0
23. Schmitz SA, Taupitz M, Wagner S, Wolf KJ, Beyersdorff D, Hamm B (2001) Magnetic resonance imaging of atherosclerotic plaques using superparamagnetic iron oxide particles. J Magn Reson Imaging 14:355–361. doi:10.1002/jmri.1194
24. Schmitz SA, Winterhalter S, Schiffler S, Gust R, Wagner S, Kresse M, Coupland SE, Semmler W, Wolf KJ (2001) USPIO-enhanced direct MR imaging of thrombus: preclinical evaluation in rabbits. Radiology 221:237–243. doi:10.1148/radiol.2211001632
25. Sigovan M, Boussel L, Sulaiman A, Sappey-Marinier D, Alsaid H, Desbleds-Mansard C, Ibarrola D, Gamondes D, Corot C, Lancelot E, Raynaud JS, Vives V, Lacledere C, Violas X, Douek PC, Canet-Soulas E (2009) Rapid-clearance iron nanoparticles for inflammation imaging of atherosclerotic plaque: initial experience in animal model. Radiology 252:401–409. doi:10.1148/radiol.2522081484
26. Soenen SJ, Himmelreich U, Nuytten N, De Cuyper M (2011) Cytotoxic effects of iron oxide nanoparticles and implications for safety in cell labelling. Biomaterials 32:195–205. doi:10.1016/j.biomaterials.2010.08.075
27. Soenen SJ, Illyes E, Vercauteren D, Braeckmans K, Majer Z, De Smedt SC, De Cuyper M (2009) The role of nanoparticle concentration-dependent induction of cellular stress in the internalization of non-toxic cationic magnetoliposomes. Biomaterials 30:6803–6813. doi:10.1016/j.biomaterials.2009.08.050
28. Soenen SJ, Nuytten N, De Meyer SF, De Smedt SC, De Cuyper M (2010) High intracellular iron oxide nanoparticle concentrations affect cellular cytoskeleton and focal adhesion kinase-mediated signaling. Small 6:832–842. doi:10.1002/smll.200902084
29. Sosnovik DE, Nahrendorf M, Weissleder R (2008) Magnetic nanoparticles for MR imaging: agents, techniques and cardiovascular applications. Basic Res Cardiol 103:122–130. doi:10.1007/s00395-008-0710-7
30. Tang TY, Howarth SP, Miller SR, Graves MJ, Patterson AJ, U-King-Im JM, Li ZY, Walsh SR, Brown AP, Kirkpatrick PJ, Warburton EA, Hayes PD, Varty K, Boyle JR, Gaunt ME, Zalewski A, Gillard JH (2009) The ATHEROMA (Atorvastatin Therapy: Effects on Reduction of Macrophage Activity) Study. Evaluation using ultrasmall superparamagnetic iron oxide-enhanced magnetic resonance imaging in carotid disease. J Am Coll Cardiol 53:2039–2050. doi:10.1016/j.jacc.2009.03.018
31. Tang TY, Muller KH, Graves MJ, Li ZY, Walsh SR, Young V, Sadat U, Howarth SP, Gillard JH (2009) Iron oxide particles for atheroma imaging. Arterioscler Thromb Vasc Biol 29:1001–1008. doi:10.1161/ATVBAHA.108.165514
32. Taupitz M, Wagner S, Schnorr J, Kravec I, Pilgrimm H, Bergmann-Fritsch H, Hamm B (2004) Phase I clinical evaluation of citrate-coated monocrystalline very small superparamagnetic iron oxide particles as a new contrast medium for magnetic resonance imaging. Invest Radiol 39:394–405. doi:10.1097/01.rli.0000129472.45832.b0
33. Trivedi RA, Mallawarachi C, U-King-Im JM, Graves MJ, Horsley J, Goddard MJ, Brown A, Wang L, Kirkpatrick PJ, Brown J, Gillard JH (2006) Identifying inflamed carotid plaques using in vivo USPIO-enhanced MR imaging to label plaque macrophages. Arterioscler Thromb Vasc Biol 26:1601–1606. doi:10.1161/01.ATV.0000222920.59760.df
34. Trivedi RA, U-King-Im JM, Graves MJ, Kirkpatrick PJ, Gillard JH (2004) Noninvasive imaging of carotid plaque inflammation. Neurology 63:187–188. doi:10.1212/01.WNL.0000132962.12841.1D
35. Van Herck JL, De Meyer GR, Martinet W, Salgado RA, Shivalkar B, De Mondt R, Van De Ven H, Ludwig A, Van Der Veken P, Van Vaeck L, Bult H, Herman AG, Vrints CJ (2010) Multi-slice computed tomography with N1177 identifies ruptured atherosclerotic plaques in rabbits. Basic Res Cardiol 105:51–59. doi:10.1007/s00395-009-0052-0
36. Vats N, Wilhelm C, Rautou PE, Poirier-Quinot M, Pechoux C, Devue C, Boulanger CM, Gazeau F (2010) Magnetic tagging of cell-derived microparticles: new prospects for imaging and manipulation of these mediators of biological information. Nanomedicine (Lond) 5:727–738. doi:10.2217/nnm.10.44
37. Wagner M, Wagner S, Schnorr J, Schellenberger E, Kivelitz D, Krug L, Dewey M, Laule M, Hamm B, Taupitz M (2011) Coronary MR angiography using citrate-coated very small superparamagnetic iron oxide particles as blood-pool contrast agent: initial experience in humans. J Magn Reson Imaging 34:816–823. doi:10.1002/jmri.22683

38. Wagner S, Schnorr J, Pilgrimm H, Hamm B, Taupitz M (2002) Monomer-coated very small superparamagnetic iron oxide particles as contrast medium for magnetic resonance imaging: preclinical in vivo characterization. Invest Radiol 37:167–177
39. Whiteman P (1973) The quantitative measurement of Alcian Blue-glycosaminoglycan complexes. Biochem J 131:343–350
40. Yamagata T, Saito H, Habuchi O, Suzuki S (1968) Purification and properties of bacterial chondroitinases and chondrosulfatases. J Biol Chem 243:1523–1535